Available online at www.sciencedirect.com
ScienceDirect
Journal of Magnesium and Alloys xxx (xxxx) xxx
www.elsevier.com/locate/jma

Full Length Article

Designing strategy for corrosion-resistant Mg alloys based on film-free and film-covered models

Pengyu Zhao[a], Tao Ying[a,*], Fuyong Cao[b], Xiaoqin Zeng[a,*], Wenjiang Ding[a]

[a] National Engineering Research Center of Light Alloys, Shanghai Jiao Tong University, Shanghai 200240, PR China
[b] Center for Marine Materials Corrosion and Protection, College of Materials, Xiamen University, 361005, PR China

Received 23 March 2021; received in revised form 28 July 2021; accepted 1 September 2021
Available online xxx

Abstract

Mathematical models were proposed to clarify the effect of alloying on corrosion of magnesium alloys based on film-free and film-covered status. The models are applicable to explain the "barrier effect" by cathodes and the "analogous Hall-Petch relationship" between corrosion rates and grain size. The slope of corrosion rates versus alloying content is determined by the dissolution ability of film-free substrate and the hindering effects by corrosion product film. Designing strategy for corrosion-resistant Mg alloys is established.

Keywords: Magnesium; Corrosion; Modeling; Electrochemistry.

1. Introduction

Magnesium (Mg) alloys receive increasing interest as engineering and biomedical materials, owing to their high strength-to-weight ratio, good mechanical properties and excellent biocompatibility [1,2]. Nevertheless, Mg possesses a low standard electrode potential, acting as an extremely active metal [3]. It will readily form a micro-galvanic corrosion system with secondary phases [4], impurities [5,6] and even grain boundaries [7,8], leading to a poor corrosion resistance in aqueous environment [9]. Therefore, the greatest obstacle in the application of Mg alloys is to address the corrosion problem.

The worldwide researchers have attempted to unravel the influencing factors of micro-galvanic corrosion, e.g. grain size [10–12], impurity concentration [13], texture [14,15], processing techniques [16,17], and environmental factors [18]. Liu and Schlesinger [19] proposed a micro-galvanic cell model and calculated the average current based on Tafel type kinetics. Ralston et al. [10] and Gollapudi [8] suggested the Hall–Petch type relationship between grain size and corrosion rates, depending upon the ability of alloying elements to passivate or activate in environment. Liu and Song [5] investigated the tolerance limit of Fe impurity in Mg alloy and attribute it to the precipitation of the Fe rich phase. Although some studies are conducted to investigate the relationship between alloying and corrosion, the detailed numerical or theoretical modeling to express the micro-galvanic corrosion is rather limited.

Besides the influence of micro-galvanic corrosion, corrosion product film is also a critical parameter in determining the corrosion behavior of Mg alloys. In general, the corrosion product film tends to cover the surface of Mg alloys and generate hindering effects. Xu et al. [20] reported Mg-Li-based alloys possessed incredibly low corrosion rates (<0.2 mm/y), with the formation of an impervious lithium carbonate film. Deng [9] designed Mg–Ca alloys showed corrosion rates lower than 0.25 mm/y in NaCl solution, possessing a protective film by Ca micro-alloying. Apparently, the product film is indeed critical in corrosion of Mg alloys, but the underlying mechanism is still unclear [21].

Therefore, mathematical models are established to interpret the effect of micro-galvanic cells and the product film on

* Corresponding authors.
E-mail addresses: yingtao85@sjtu.edu.cn (T. Ying), xqzeng@sjtu.edu.cn (X. Zeng).

https://doi.org/10.1016/j.jma.2021.09.003

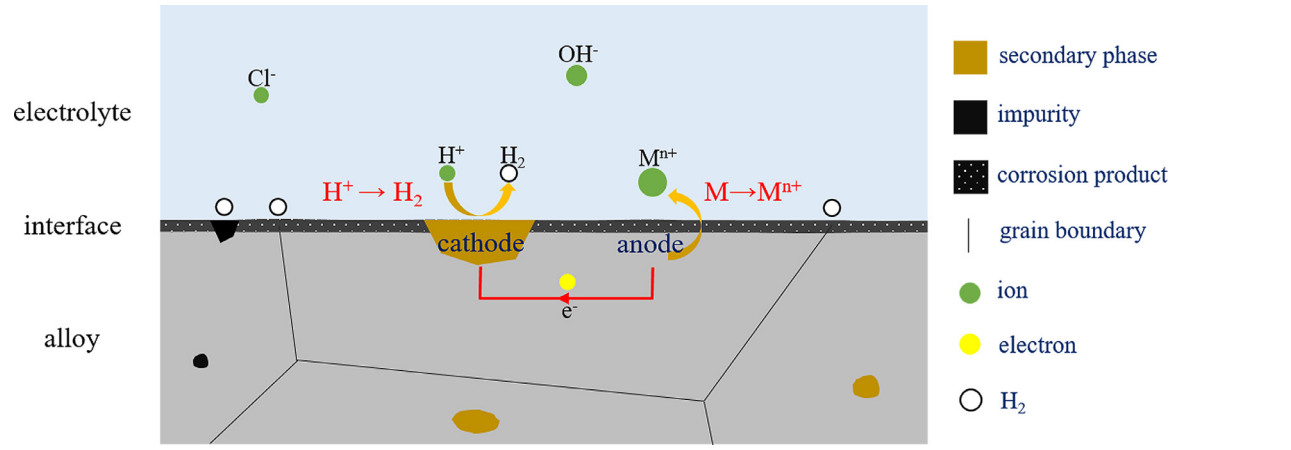

Fig. 1. Micro-galvanic cells depiction of the corrosion process.

corrosion, so as to reveal the influence of alloying element's concentration, distribution of secondary phases (or element accumulation areas, impurities) and grain size on corrosion rates. Based on the models, a designing strategy of corrosion-resistant Mg alloys is developed.

2. Problem formulation

The corrosion of Mg alloys is usually caused by the micro-galvanic cells of Mg matrix and second phases or impurities, which is highly sensitive to the microstructure and composition. With the proceeding of corrosion, the corrosion products would simultaneously deposit and accumulate on the surface, providing hindering effects. Therefore, the corrosion behavior of Mg alloys is separately discussed from film-free and film-covered status. The film-free status refers to the dissolution of anode without consideration of corrosion product, while the film-covered status aggregates the hindering effects on the dissolution process owing to the protectiveness of the corrosion products. As illustrated in Fig. 1, micro-galvanic cells would form among various microscale structures, such as Mg matrix, secondary phases, impurities and grain boundaries, leading to the initiation of micro-galvanic corrosion. However, with the formation of corrosion product film, corrosion process is retarded, thus the actual corrosion behavior is determined by the competition of the dissolution ability of film-free substrate and the hindering effects by corrosion product film. The actual current density, i, can be expressed in a quantitative way:

$$i = i^{ff} - i^{he} \tag{1}$$

where i^{ff} is the current density attributed from the dissolution ability of film-free substrate. It is worth noting that i^{he} represents the current density of the hindering effects from corrosion product film, which is not the real current passing through the film-covered area.

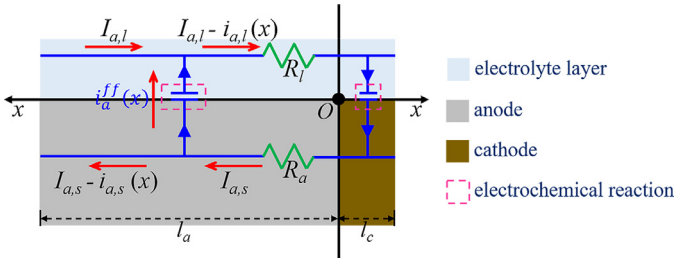

Fig. 2. Schematic plot of one dimensional micro-galvanic cell.

2.1. Film-free model

To elucidate the film-free model, a simplified micro-galvanic cell model was established in Fig. 2. The micro-galvanic cell can be depicted as a transmission line consisting of an anode and a cathode in a thin electrolyte layer [22]. The following assumptions have been made in the current work: (1) Electrolyte solution is well mixed and no concentration gradient exists in the electrolyte solution. (2) The solution is electro neutral. (3) The composition of the anode and cathode are evenly distributed. (4) Dissolution reaction takes place at the anode surface whereas hydrogen evolution reaction takes place at the cathode surface. (5) The electrochemical reactions of the interface between the electrolyte and electrode follow the Tafel kinetics [19,23].

In the electrochemical process, electrons currents always flow out from an anode and flow into a cathode. The total anodic current $i^{ff}_{a,total}$ and total cathodic current $i^{ff}_{c,total}$ satisfy the following equation [19]:

$$i^{ff}_{a,total} + i^{ff}_{c,total} = 0 \tag{2}$$

The subscript a and c represents anode and cathode correspondingly, and the superscript ff represents the film-free status to distinguish from the film-covered status discussed below. The current density of film-free status i^{ff} equals to $i^{ff}_{a,total}$ divided by $(l_a + l_c)$, where l_a and l_c are the length of

anode and cathode as shown in Fig. 2.

$$i^{ff} = \frac{i^{ff}_{a,total}}{l_a + l_c} = -\frac{i^{ff}_{c,total}}{l_a + l_c} \tag{3}$$

$i^{ff}_{a,total}$ can be obtained by integrating anodic current density $i^{ff}_a(x)$ [22,24,25]

$$i^{ff}_{a,total} = \int_0^{l_a} i^{ff}_a(x) \cdot dx \tag{4}$$

Hereinto, $i^{ff}_a(x)$ can be expressed as (calculation details see Appendix A)):

$$i^{ff}_a(x) = \frac{1}{m(R_l + R_a)} \frac{1}{x - C_a} \tag{5}$$

where R_l and R_a are the solution resistance of the electrolyte and the metal resistance of anode per unit length, which are x independent constants. C_a (<0, detailed values see Appendix A) is the integral constant determined by the type of electrode and electrolyte, $m = \frac{z_a \gamma_a F}{RT}$, z is the valence, γ is the symmetry factor, F is the Faraday's constant, R is the universal gas constant, T is absolute temperature. Similarly, $i^{ff}_{c,total}$ and $i^{ff}_c(x)$ can be obtained as follows:

$$i^{ff}_{c,total} = \int_0^{l_c} i^{ff}_c(x) \cdot dx \tag{6}$$

$$i^{ff}_c(x) = \frac{1}{n(R_l + R_c)} \frac{1}{x - C_c} \tag{7}$$

where R_c is the metal resistance of cathode per unit length. C_c (<0, detailed values see Appendix A) is the integral constant, $n = -\frac{z_c(1-\gamma_c)F}{RT}$.

Finally, the current density of film-free status i^{ff} can be expressed as:

$$i^{ff} = \frac{l_a}{l_a + l_c} \left(\frac{l_c}{l_a}\right)^N \cdot i_{a,corr} exp\left[k^{ff}\ (\varphi_{c,corr} - \varphi_{a,corr}) + b^{ff}\right] \tag{8}$$

where $N = \frac{z_a \gamma_a}{z_a \gamma_a + z_c(1-\gamma_c)}$, $k^{ff} = m(1 - N)$, $b^{ff} = Nln\frac{i_{c,corr}}{i_{a,corr}}$. $i_{a,corr}(i_{c,corr})$ and $\phi_{a,corr}(\phi_{c,corr})$ are the corrosion current density and corrosion potential of anode (cathode). Assume $k_m = \frac{l_a}{l_a + l_c}(\frac{l_c}{l_a})^N$, $i^*_a = i_{a,corr} exp[k^{ff}\ (\varphi_{c,corr} - \varphi_{a,corr}) + b^{ff}]$, i^{ff} can be expressed as:

$$i^{ff} = k_m i^*_a \tag{9}$$

Apparently, k_m is a structural factor determined by the distribution of anodes and cathodes, and i^*_a is positively correlated to the potential difference between anodes and cathodes ($\phi_{c,corr} - \phi_{a,corr}$).

It is worth noting that other factors, such as cathodic catalytic effect [21] and poisoning effects of the addition of arsenic (As) to Mg [26], would also affect the micro-galvanic corrosion of Mg alloys, which requires future work to clarify and thus not incorporated in the current model.

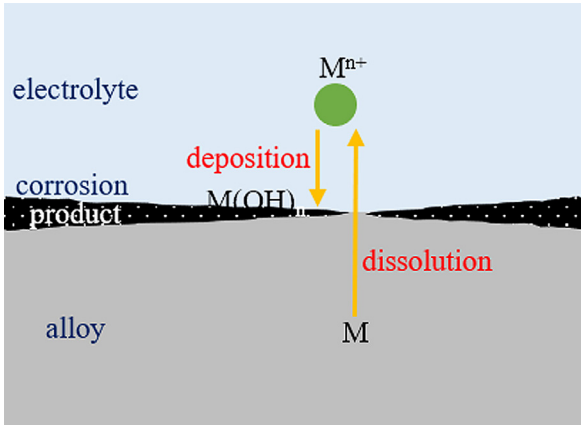

Fig. 3. Schematic plot of the formation process of corrosion product film.

2.2. Film-covered model

As illustrated in Fig. 3, the metal cations M^{n+} released by the dissolution process of film-free status is capable to deposit on the interface by forming corrosion products $M(OH)_n$. Ignoring the dissolution of corrosion products, the formation of $M(OH)_n$ can be expressed as formula (10).

$$M^{n+} + nOH^- \rightarrow M(OH)_n \tag{10}$$

The corrosion products would produce the hindering effects on the corrosion behavior of film-covered status. The current density attributed from the hindering effects by corrosion product film i^{he} is mainly proportional to the resistance of corrosion products R_{cp}. R_{cp} attributes to the inhibition efficiency, generally determined by three critical parameters. (1) The supersaturation of metallic cation M^{n+} generating from the dissolution of alloys, $(\frac{c_{M^{n+}} c^n_{OH^-}}{K_{sp}})$, associated with the driving force of forming corrosion products. (2) The nucleation density and growth rate of the corrosion product film, k_r, corresponding to the crystallization process and the growth quality of the film. (3) The compactness level of corrosion products, k_c, indicating the ability of providing the protectiveness. Hence, R_{cp} can be expressed as:

$$R_{cp} \propto \left(\frac{c_{M^{n+}} c^n_{OH^-}}{K_{sp}}\right) k_r k_c \tag{11}$$

where k_c is related to the Pilling-Bedworth ratio (PBr) [27,28], k_r is considered as a function of Gibbs energies of formation ($\Delta_f G^o$) [27], K_{sp} is solubility product constants, $c_{M^{n+}}$, c_{OH^-} are the concentration of M^{n+} and OH^- in the interface, respectively. According to the Faraday law [29], the concentration of $c_{M^{n+}}$ generating from the corrosion of alloys can be presented as:

$$c_{M^{n+}} = \frac{i^{ff}}{nF\delta} \tag{12}$$

where δ is the thickness of diffusion layer. As the inhibiting effect is positively dependent on R_{cp}, we assume i^{he} is proportional to R_{cp}. Therefore, i^{he} can be expressed as:

$$i^{he} = k^{he} i^{ff} + b' \tag{13}$$

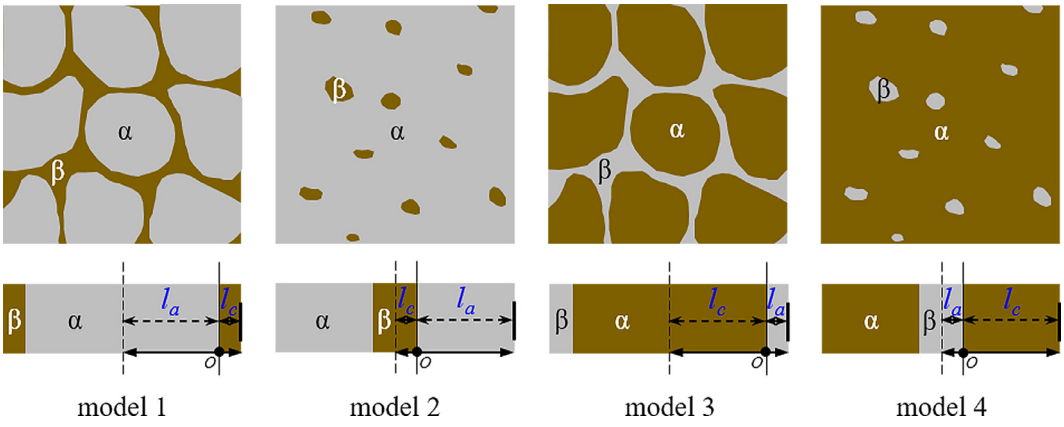

Fig. 4. Schematic diagram of four typical distribution models.

where $k^{he} = \frac{k' k_r k_c c_{OH^-}^n}{k_{sp} n F \delta}$, k' and b' are proportionality coefficients.

Finally, the actual current density, i, can be calculated by substituting Eq. (13) into Eq. (1).

$$i = \left(1 - k^{he}\right) i^{ff} - b' \tag{14}$$

3. Results and discussion

3.1. Microstructure and composition

Microstructure and composition are the intrinsic characteristics of alloys, which play a determining role in the corrosion behavior. Herein, based on the abovementioned models, the influences of microstructure and composition on the corrosion were discussed from three perspectives: distribution of anode and cathode, grain size and the composition.

3.1.1. Anode and cathode distribution

Regarding to the reported microstructure of Mg alloys, there are four typical distribution types: (1) continuous cathode nets (model 1) [30], dispersed cathode particles (model 2) [31], continuous anode nets (model 3) [3] and dispersed anode particles (model 4) [32]. Four models were correspondingly set up as depicted in Fig. 4. Considering the micro-galvanic cell as concentric circles in a binary Mg-wA alloy, composed of α phase and β phase, the corrosion current density can be calculated based on the *Film-free model*. Herein, the total weight percentage of alloying, w, is

$$w = \frac{S_\alpha \rho_\alpha w_\alpha + S_\beta \rho_\beta w_\beta}{S_\alpha \rho_\alpha + S_\beta \rho_\beta} \tag{15}$$

The subscript α and β represent the α phase and β phase correspondingly. ρ, w and S are the density, weight percentage and aera of the phases.

The relationship between i^{ff} and w of the four models were plotted in Fig. 5 (detailed parameters for calculation see Appendix B, Table. B1). In terms of the film-free status, the i^{ff} increases monotonously with the increment of w. When the type of distribution (k_m, see Eq. (9)) is the same, the corrosion current density of cathode model (model 1 and 2) is substantially lower than that of anode model (model 3 and 4). For example, although the anode or cathode are both haphazardly dispersed, the corrosion current density of anode model (model 4) is three times of that in cathode model (model 2). This result is consistent with the well-known "large cathode connected to a small anode" effect, which would accelerate the corrosion process [33]. In addition, the corrosion rate is the lowest when the cathode distributed in continuous nets, as displayed in model 1. The cathode nets are able to exert the so-called "barrier effect", preventing the deep corrosion of Mg, so as to lower the corrosion rates in alloying systems like Mg-Al series [30,34].

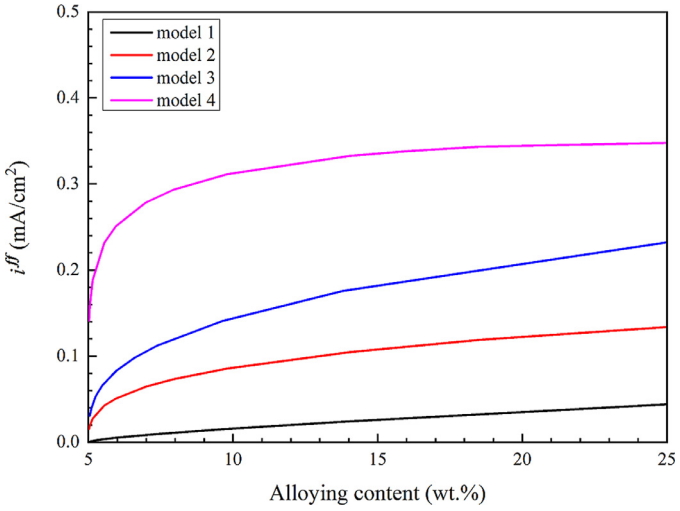

Fig. 5. Relationship between i^{ff} and w of the four investigated models.

3.1.2. Grain size

It is worth noting the model 1 can be extended to depict the effect of grain size d on corrosion rate, where the grain boundaries could be considered as cathode nets with the size of l_c. Here, $d = 2(l_a + l_c)$, and $l_c \ll l_a$. Combining with Eqs. (9) and (14), i can be expressed as:

$$i = \left(1 - k^{he}\right) i_a^* k_m - b' \tag{16}$$

Table. 1
Corrosion potential ϕ_{corr} of intermetallic phases (or pure metals) in 0.1 M NaCl, $\Delta_f G^o$, pK_{sp}, k_c and valence n corresponding to the oxides, hydroxides and metallic cations of the alloy systems [4,37,38].

Alloy system	ϕ_{corr} (V$_{SCE}$)	$\Delta_f G^o$ (kJ/mol)	pK_{sp}	k_c	n
Mg	−1.65 (Mg)	−569.3(MgO)	11.25($Mg(OH)_2$)	0.80 (MgO)	2
Mg-Ca	−1.75 (Mg_2Ca)	−603.3 (CaO)	5.26 ($Ca(OH)_2$)	0.64 (CaO)	2
Mg-Al	−1.35 ($Mg_{17}Al_{12}$)	−1582.3 (Al_2O_3)	32.89 ($Al(OH)_3$)	1.28 (Al_2O_3)	3
Mg-Mn	−1.28 (Mn)	−362.9 (MnO)	12.72 ($Mn(OH)_2$)	1.23 (MnO)	2
Mg-Zn	−1.03 ($MgZn_2$)	−320.5 (ZnO)	16.50 ($Zn(OH)_2$)	1.42 (ZnO)	2
Mg-Fe	−0.60 (Fe)	−251.4 (FeO)	16.31 ($Fe(OH)_2$)	1.22 (FeO)	2
Mg-Ni	−0.22 (Ni)	−211.7 (NiO)	15.26 ($Ni(OH)_2$)	1.30 (NiO)	2
Mg-Cu	−0.15 (Cu)	−129.7 (CuO)	19.66 ($Cu(OH)_2$)	1.28 (CuO)	2
Mg-Y	−1.60 ($Mg_{24}Y_5$)	−1816.7 (Y_2O_3)	22.00 ($Y(OH)_3$)	1.13 (Y_2O_3)	3
Mg-Ce	−1.50 ($Mg_{12}Ce$)	−1706.2 (Ce_2O_3)	19.80 ($Ce(OH)_3$)	1.15 (Ce_2O_3)	3
Mg-La	−1.60 ($Mg_{12}La$)	−1705.8 (La_2O_3)	18.70 ($La(OH)_3$)	1.10 (La_2O_3)	3
Mg-Nd	−1.55 (Mg_3Nd)	−1720.9 (Nd_2O_3)	21.49 ($Nd(OH)_3$)	1.13 (Nd_2O_3)	3

where only k_m is dependent of l_a and l_c, and k_m can be simplified as:

$$k_m \approx k_{gs} d^{-\frac{z_a\gamma_a}{z_a\gamma_a+z_c(1-\gamma_c)}} \tag{17}$$

Where $k_{gs} = (2l_c)^{\frac{z_a\gamma_a}{z_a\gamma_a+z_c(1-\gamma_c)}}$. Accordingly, the relationship between corrosion rate i and grain size d can be expressed analogously to the Hall-Petch effect:

$$i = A + Bd^{-p} \tag{18}$$

where $A = -b'$, $B \approx (1-k^{he})k_{gs}i_a^*$, $p = \frac{z_a\gamma_a}{z_a\gamma_a+z_c(1-\gamma_c)}$. Apparently, $0 < p < 1$.

Song et al. [35] and Ralston et al. [36] studied the effect of grain size on corrosion rate of pure Mg and pure Al possessing lower and relatively higher corrosion resistance, respectively. They also discovered the similar Hall–Petch relationship of corrosion rate and grain size, which validates the correct of our mathematical model.

3.1.3. Composition

Besides the aforementioned two factors, the composition is also a critical parameter in governing the corrosion behavior. As the role of alloying elements on film-covered status is the competition results of the dissolution ability of film-free substrate and the hindering effects by corrosion product film, the i^{ff}/i^{he} of different elements are calculated and compared with pure Mg. Detailed calculation parameters is listed in Table 1 [4,37,38], and other information of calculation process see Appendix C. As shown in Fig. 6, the i^{ff}/i^{he} values of Fe, Cu and Ni are much higher than other elements, id est, exhibit significantly higher tendency to corrode. As for the commonly used elements in commercial alloys, e.g. Al, Zn and Mn, the dissolution ability of film-free substrate and the hindering effects by corrosion product film both enhanced, but the ratio of i^{ff}/i^{he} decreased, especially in the case of Al. It is interesting to note that all the calculated RE elements perform relatively low values of i^{ff}/i^{he}, indicating the addition of RE elements would be benefit to improve the corrosion resistance of Mg alloys.

To further analyze and testify the result of calculation, the actual corrosion rates of different binary Mg-X alloys in 3.5 wt.% NaCl solution were plotted in Fig. 7, data are

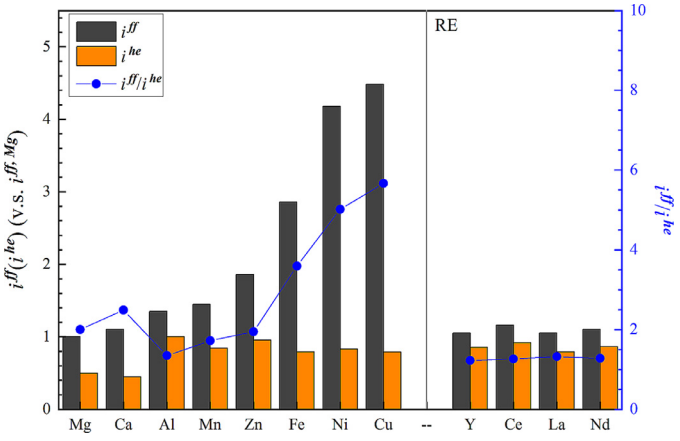

Fig. 6. i^{ff}, i^{he} and i^{ff}/i^{he} values relative to pure Mg of different alloy systems.

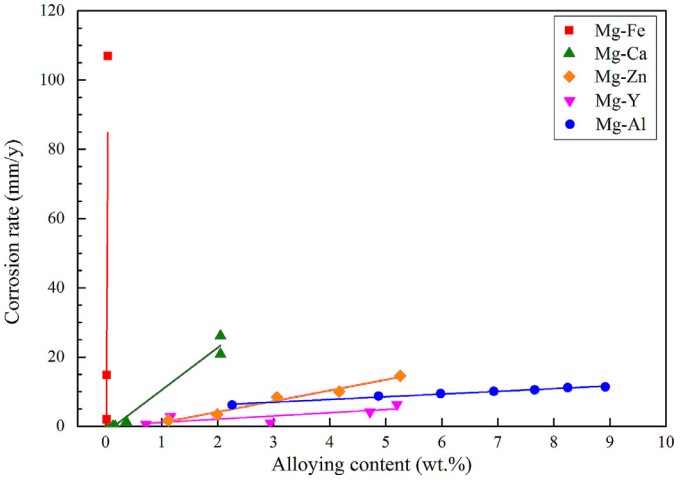

Fig. 7. Relationship between corrosion rates and alloying content of binary Mg-X (X = Fe, Ca, Zn, Y, Al) alloys in 3.5 wt.% NaCl solution [9,13,32,39–43].

from Refs. [9,13,32,39–43]. With the increasing of the alloying contents, the corrosion accelerates, which implies the hindering effects by corrosion product film is not comparable to the dissolution ability of film-free substrate in most binary Mg alloys. It is worth noting that the slope of corrosion rates

versus alloying content ($k_{cr/ac}$) shows distinct discrepancy in different alloying systems. For instance, the corrosion rates increase dramatically with the addition of Fe, Cu, and Ni, while the growth of corrosion rates is slow in Mg-Al and Mg-Y alloys.

More importantly, the dependence of alloying content with corrosion rate is closely related to i^{ff}/i^{he}. As displayed in Fig. 8, $k_{cr/ac}$ is positively correlated to i^{ff}/i^{he}. The higher i^{ff}/i^{he}, the larger increment of corrosion rate by alloying, and vice versa. For example, the Fe element, whose i^{ff}/i^{he} values are the highest, shows a catastrophic anti-corrosion performance when adding to Mg. Nevertheless, when adding the elements with small i^{ff}/i^{he} like Al or Y, the corrosion is relatively weak, leading to a low corrosion rate. The ranking of the growth rate of corrosion rate/alloying content is summarized as follows:Fe >> Ca > Zn > Al ≈ *Y*, which is analogous to the variation of i^{ff}/i^{he}, suggesting the accuracy of the proposed mathematical models.

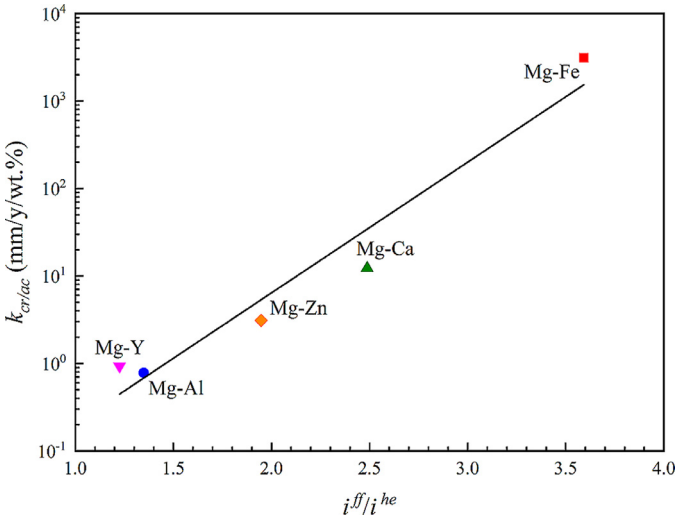

Fig. 8. Relationship between i^{ff}/i^{he} and $k_{cr/ac}$ for binary Mg-X (Fe, Ca, Zn, Y, Al) alloys.

3.2. Corrosion-resistant mg alloy designing strategy

Although several corrosion-resistant Mg alloys were discovered occasionally by worldwide researchers [3,9,44–47], there is little consensus as to a designing strategy applicable to Mg alloys. Based on the proposed models, three selective criteria for alloying elements are established as follows:

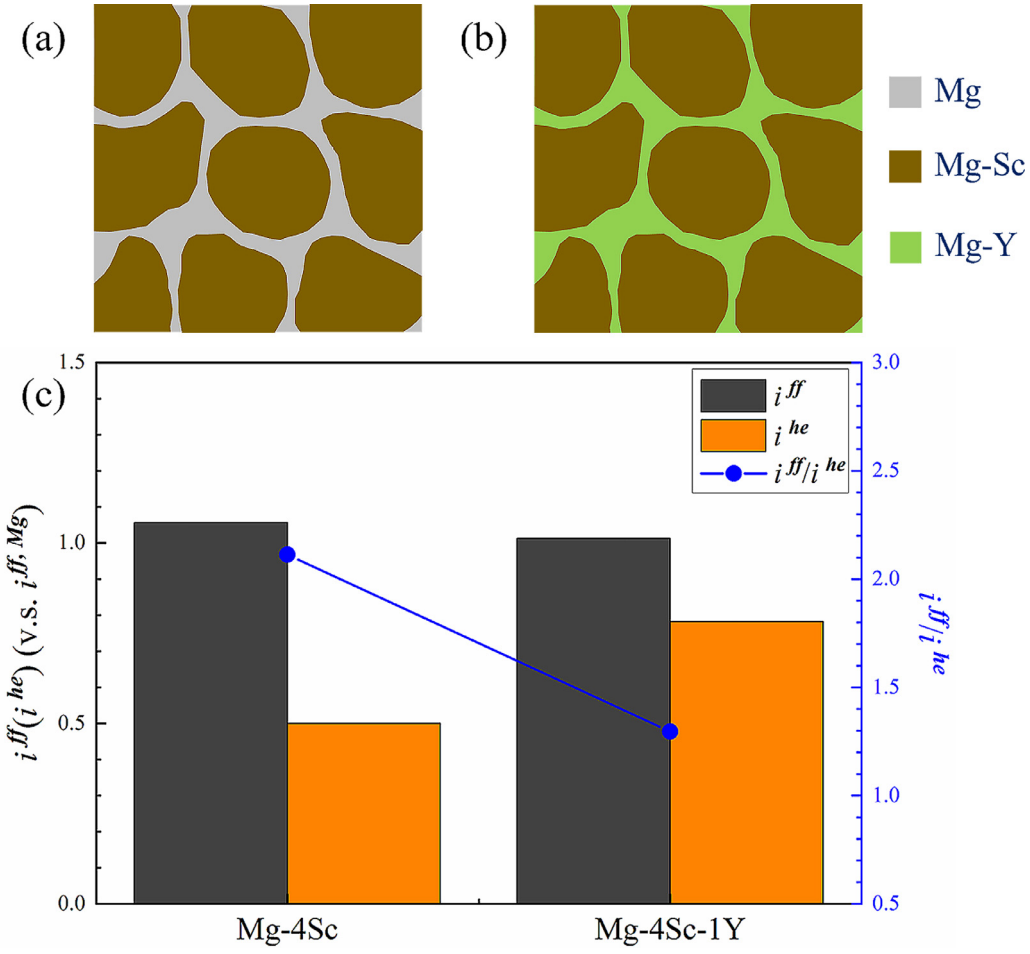

Fig. 9. Microstructure schematic plots of (a) Mg-4Sc and (b) Mg-4Sc-1Y alloy with (c) correspondingly i^{ff}, i^{he} and i^{ff}/i^{he} values relative to pure Mg.

Table. 2
Corrosion potential difference ($\phi_{c,corr} - \phi_{a,corr}$), $\Delta_f G^o$, pK_{sp}, k_c and valence n corresponding to the oxides, hydroxides and metallic cations of the alloy systems [3,37].

Alloy system	$\phi_{c,corr} - \phi_{a,corr}$ (mV)	$\Delta_f G^o$ (mA/cm^2) (kJ/mol)	pK_{sp}	k_c	n
Mg-*Sc*	55	−569.3(MgO)	11.25($Mg(OH)_2$)	0.80 (MgO)	2
Mg-*Sc*-Y	13	−1816.7 (Y_2O_3)	22.00 ($Y(OH)_3$)	1.13 (Y_2O_3)	3

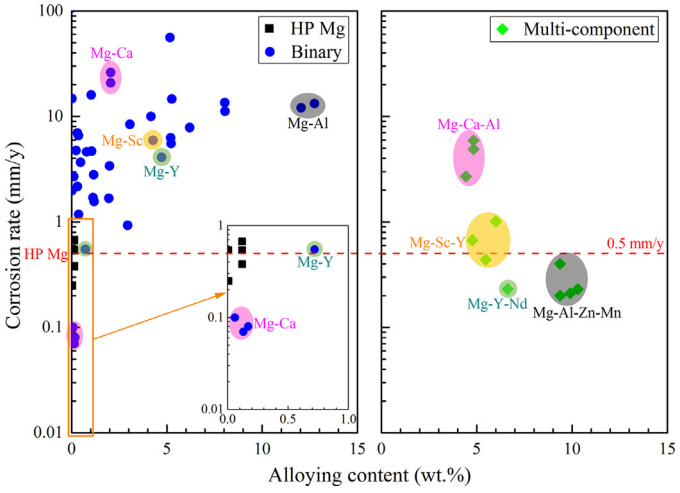

Fig. 10. Corrosion rates of HP Mg, binary and multicompetent Mg alloys in solutions similar to 3.5 wt.% NaCl include 3.5 wt.% and 5 wt.% NaCl saturated with $Mg(OH)_2$, 3 wt.% NaCl, 0.6 M NaCl aqueous solutions. Data collected from literature [3,9,13,30,39–62].

(1) Decreasing the potential difference between anodes and cathodes ($\phi_{c,corr} - \phi_{a,corr}$) to reduce the dissolution ability of film-free substrate.
(2) Producing a more protective corrosion product film with a smaller K_{sp}, more negative $\Delta_f G^o$ and PBr > 1 to enhance the hindering effects.
(3) Regulating the cathodes distribution as continuous nets or dispersed particles.

By controlling the up-mentioned three criteria, corrosion-resistant Mg alloys could be developed. Use the Mg-*Sc* alloy as the example (Fig. 9 and Table 2), the addition of Y into peritectic Mg-4 wt.%*Sc* alloy could considerably lower the potential difference from 55 mV to 13 mV, thereby decreasing the dissolution ability of film-free substrate i^{ff}. Moreover, the formation of yttrium oxide is helpful to increase the $\Delta_f G^o$, pK_{sp} and k_c, which would contribute to improving the compactness and protection of the corrosion product film. Thus, the stronger hindering effects i^{he} would be provided with Y addition. Accordingly, the value of i^{ff}/i^{he} decrease dramatically, and the actual corrosion rate of the film-covered status in Mg-4Sc-1Y ternary alloy is only one tenth of that in Mg-4Sc alloy as reported in Ref. [3].

To further verify the designing strategy, the corrosion rate of reported Mg alloys [3,9,13,30,39–62] have been summarized and depicted as Fig. 10. In terms of binary Mg alloys, as nearly all the alloying elements produce a stronger dissolution ability of film-free substrate than the hindering effects by corrosion product film, it is difficult for binary Mg alloys to exhibit a lower corrosion resistance than high-purity (HP) Mg. Only through micro-alloying (alloying content < 1%), the corrosion rate is possible to maintain the same level or even lower than HP Mg, such as Mg-Ca [9] and Mg-Y alloys [41]. However, the mechanical properties of these alloys are usually poor due to the absence of intermetallic compounds. With the further increase of alloying concentration in binary Mg alloys, the corrosion rates are substantially higher than HP Mg, which is attributed to the weaker tendency of forming a protective corrosion product film comparable to the dissolution ability of film-free substrate.

As for the multi-component Mg alloys, the main alloying element should possess a low value of i^{ff}/i^{he}, and other elements have the ability to inhibit the dissolution ability of the major element in film-free substrate or/and enhance the hindering effects by forming a more protective corrosion product film. For instance, the corrosion rate of binary Mg-2Ca is as high as 20 mm/y. From the perspectives of designing strategy, element Al is capable to depress the dissolution ability of the substrate with Mg_2Ca phase [32], forming a protective film to hinder corrosion [63] and alter the microstructure [64]. Therefore, Al satisfies the designing strategy and is expected to improve the corrosion behavior of Mg-2Ca. In fact, the corrosion rate of ternary Mg-2Ca-2Al alloy did decrease to 5 mm/y. Similar strategy is also applicable to other systems, e.g. adding Nd to Mg-Y alloys [41,46], adding Zn and Mn to Mg-Al alloys [5,30,40,45,65–67].

Based on the designing strategy to lower i^{ff}/i^{he}, high corrosion-resistant Mg alloys can be developed. As for binary Mg alloys, micro-alloying is the key to suppress the dissolution ability of the film-free substrate. In regard to multi-component Mg alloys, a passive-led major element with minor other elements to improve the hindering effects by corrosion product film and/or depress the dissolution ability of the film-free substrate are workable as well.

4. Conclusion

The addition of alloying elements always brings about the modification of microstructure, composition, and corrosion product film, consequently affecting the corrosion behavior. Mathematical models were proposed to clarify the role of alloying on film-free and film-covered corrosion. The main conclusions are as follows:

(1) Mathematical models were established to clarify the micro-galvanic corrosion behavior depending on film-free and film-covered status. The models explained the

Table. B1
Detailed parameter values for calculating the corrosion current density (i^{ff}) and w in a binary Mg-wA alloy.

	electrode (phase)	ϕ_{corr} (V) (V_{SCE})	i_{corr} (mA/cm^2)	z	γ	ρ(g/cm^3)	w
model 1(2)	anode (α)	−1.50	0.010	2	0.5	1.7	0.05
	cathode (β)	−1.20	0.005	1	0.5	5.2	0.75
model 3(4)	cathode (α)	−1.50	0.010	2	0.5	1.7	0.05
	anode (β)	−1.80	0.020	1	0.5	5.2	0.75

influence of secondary phases (or element accumulation areas, impurities) distribution on corrosion rates, and among the four typical distribution models with certain alloying contents, the cathodes forming a continuous-net exhibit the lowest corrosion rate.
(2) The analogous Hall-Petch relationship between corrosion rate and grain size can be well interpreted by the film-free and film-covered models.
(3) The slope of corrosion rates versus alloying content is positively correlated to the corrosion current density ratio of film-free to film-covered status.
(4) Designing strategy of high corrosion-resistant alloys is proposed and validated in Mg alloys. Weakening the dissolution ability of film-free substrate and enhancing the hindering effects by corrosion product film are the key factors that should be controlled.

Data availability

The raw/processed data required to reproduce these findings cannot be shared at this time as the data also forms part of an ongoing study.

Declaration of Competing Interest

The authors declare that they have no known competing financial interests or personal relationships that could have appeared to influence the work reported in this paper.

Acknowledgments

This work was supported by Shanghai Science and Technology Committee (No. 18511109300), Science and Technology Commission of the CMC (2019JCJQZD27300), Foundation from Shanghai Jiao Tong University (AF0500132, AF0500149), Funding from Center of Hydrogen Science of Shanghai Jiao Tong University.

Appendix A. Calculation of $i_a^{ff}(x)$ and $i_c^{ff}(x)$

Suppose R_l is the solution resistance per unit length of the electrolyte, and R_a the metal resistance of the anode. R_l and R_a are x independent constants, representing the resistances per unit length. The voltage drop (Ohmic drop) of an infinitesimal length dx is expressed by the following differential equations [22,24–25].

$$-d\varphi_{a,l}(x) = i_{a,l}(x)R_l dx \tag{A.1}$$

$$-d\varphi_{a,s}(x) = i_{a,s}(x)R_a dx \tag{A.2}$$

Where $\phi_{a,l}(x)$, $i_{a,l}(x)$ are the potential and current of the electrolyte (subscript l represents liquid, a represents anode) in position x, and $\phi_{a,s}(x)$, $i_{a,s}(x)$ are the potential and current of the anode (subscript s represents solid) in position x. Suppose the electrochemical reactions in the charged interface follow the Tafel kinetics. Then the polarization relationship can be expressed as:

$$i_a(x) = i_{a,corr}exp\left[\frac{z_a\gamma_a F}{RT}\left(\varphi_{a,s}(x) - \varphi_{a,l}(x) - \varphi_{a,corr}\right)\right] \tag{A.3}$$

Where $i_{a,corr}$ is the corrosion current density of the anode, z is the valence, γ is the symmetry factor, F is the Faraday's constant, R is the universal gas constant, T is absolute temperature, $\phi_{a,corr}$ is the corrosion potential of the anode. Ignoring the mass transfer process in the electrolyte and non-Faraday process in the interface zone, the current drop at position x (see Fig. 2) of the anode would be equal to that of the electrolyte as well as the current in the interface. Hence, relationship of current in the metal, electrolyte and interface can be taken as:

$$|i_a(x)| = |i_{a,l}(x)| = \left|i_{a,s}(x)\right| \tag{A.4}$$

Combining the above equations, the anodic current distribution $i_a^{ff}(x)$ can be expressed as follows.

$$i_a^{ff}(x) = \frac{1}{m(R_l + R_a)}\frac{1}{x - C_a} \tag{A.5}$$

$$C_a = -\frac{1}{m(R_l + R_a)}\frac{1}{i_{a,corr}exp\left[m\left(\varphi_0 - \varphi_{a,corr}\right)\right]} \tag{A.6}$$

$$\varphi_0 = \frac{\frac{RT}{F}ln\frac{l_c}{l_a}\frac{i_{c,corr}}{i_{a,corr}}}{z_a\gamma_a + z_c(1-\gamma_c)} + \frac{z_c(1-\gamma_c)\varphi_{c,corr} + z_a\gamma_a\varphi_{a,corr}}{z_a\gamma_a + z_c(1-\gamma_c)} \tag{A.7}$$

Where C_a (<0) is an integral constant determined by the type of anode and electrolyte, $m = \frac{z_a\gamma_a F}{RT}$. $i_{a,corr}(i_{c,corr})$ and $\phi_{a,corr}(\phi_{c,corr})$ are the corrosion current density and corrosion potential of anode (cathode), and ϕ_0 is the electrode potential at the contact point O. Similarly, cathodic current distribution $i_c(x)$ can be expressed as:

$$i_c^{ff}(x) = \frac{1}{n(R_l + R_c)}\frac{1}{x - C_c} \tag{A.8}$$

$$C_c = -\frac{1}{n(R_l + R_c)}\frac{1}{i_{c,corr}exp\left[n\left(\varphi_0 - \varphi_{c,corr}\right)\right]} \tag{A.9}$$

Where $n = -\frac{z_c(1-\gamma_c)F}{RT}$ (subscript c represents cathode). C_c (<0) is an integral constant.

Appendix B. Appendix Table

Appendix para

Appendix C. Calculation of i^{ff}/i^{he}

Here, the related equations in Section 2 were simplified in the calculation process.

As depicted in Eq. (9), i^{ff} is mainly the function of $(\phi_{c,corr} - \phi_{a,corr})$,which can be expressed as

$$i^{ff} = exp\left(\varphi_{c,corr} - \varphi_{a,corr}\right) \tag{A.10}$$

where $\phi_{c,corr}$ and $\phi_{a,corr}$ are the corrosion potential of cathode and anode, respectively. According to the crystallization process in aqueous solution involves the formation of nucleus and their growth [68], k_r can be expressed as

$$k_r = exp\left(\frac{-\Delta_f G^o}{RT}\right) \tag{A.11}$$

where $\Delta_f G^o$ is the Gibbs energies of formation.

Additionally, $\delta = 10\ \mu$m, pH $= 12$ were assigned. k' and b' are obtained referring to Mg by assuming $i^{ff}/i^{he} = 2$.

References

[1] Z. Wu, R. Ahmad, B. Yin, S. Sandlöbes, W.A. Curtin, Mechanistic origin and prediction of enhanced ductility in magnesium alloys, Science 359 (2018) 447–452, doi:10.1126/science.aap8716.
[2] N.T. Kirkland, J. Lespagnol, N. Birbilis, M.P. Staiger, A survey of bio-corrosion rates of magnesium alloys, Corros. Sci. 52 (2010) 287–291, doi:10.1016/j.corsci.2009.09.033.
[3] P. Zhao, T. Xie, X. Xu, H. Zhu, F. Cao, T. Ying, X. Zeng, Designing high corrosion resistant peritectic magnesium alloys via *Sc* and Y addition, Metall. Mater. Trans. A Phys. Metall. Mater. Sci. 51 (2020) 2509–2522, doi:10.1007/s11661-020-05693-5.
[4] A.D. Südholz, N.T. Kirkland, R.G. Buchheit, N. Birbilis, Electrochemical properties of intermetallic phases and common impurity elements in magnesium alloys, Electrochem. Solid State Lett. 14 (2011) 2010–2012, doi:10.1149/1.3523229.
[5] M. Liu, G.L. Song, Impurity control and corrosion resistance of magnesium-aluminum alloy, Corros. Sci. 77 (2013) 143–150, doi:10.1016/j.corsci.2013.07.037.
[6] J. Yang, C. Blawert, S.V. L.amaka, K.A. Yasakau, L. Wang, D. Laipple, M. Schieda, S. Di, M.L. Zheludkevich, Corrosion inhibition of pure Mg containing a high level of iron impurity in pH neutral NaCl solution, Corros. Sci. 142 (2018) 222–237, doi:10.1016/j.corsci.2018.07.027.
[7] A. Lervik, S. Wenner, O. Lunder, C.D. Marioara, R. Holmestad, Grain boundary structures and their correlation with intergranular corrosion in an extruded Al-Mg-Si-Cu alloy, Mater. Charact. 170 (2020) 110695, doi:10.1016/j.matchar.2020.110695.
[8] S. Gollapudi, Grain size distribution effects on the corrosion behavior of materials, Corros. Sci. 62 (2012) 90–94, doi:10.1016/j.corsci.2012.04.040.
[9] M. Deng, L. Wang, D. Höche, S.V. Lamaka, C. Wang, D. Snihirova, Y. Jin, Y. Zhang, M.L. Zheludkevich, Approaching "stainless magnesium" by Ca micro-alloying, Mater. Horiz. (2021), doi:10.1039/d0mh01380c.
[10] K.D. Ralston, N. Birbilis, C.H.J. Davies, Revealing the relationship between grain size and corrosion rate of metals, Scr. Mater. 63 (2010) 1201–1204, doi:10.1016/j.scriptamat.2010.08.035.
[11] R. Mishra, R. Balasubramaniam, Effect of nanocrystalline grain size on the electrochemical and corrosion behavior of nickel, Corros. Sci. 46 (2004) 3019–3029, doi:10.1016/j.corsci.2004.04.007.
[12] W. Luo, Y. Xu, Q. Wang, P. Shi, M. Yan, Effect of grain size on corrosion of nanocrystalline copper in NaOH solution, Corros. Sci. 52 (2010) 3509–3513, doi:10.1016/j.corsci.2010.06.029.
[13] L. Yang, G. Liu, L. Ma, E. Zhang, X. Zhou, G. Thompson, Effect of iron content on the corrosion of pure magnesium: critical factor for iron tolerance limit, Corros. Sci. 139 (2018) 421–429, doi:10.1016/j.corsci.2018.04.024.
[14] G.L. Song, Z. Xu, Crystal orientation and electrochemical corrosion of polycrystalline Mg, Corros. Sci. 63 (2012) 100–112, doi:10.1016/j.corsci.2012.05.019.
[15] A. Gebert, A.A. El-Moneim, O. Gutfleisch, L. Schultz, Corrosion behavior of textured and isotropic nanocrystalline NdFeB-based magnets, IEEE Trans. Magn. 38 (2002) 2979–2981, doi:10.1109/TMAG.2002.803100.
[16] D. Orlov, K.D. Ralston, N. Birbilis, Y. Estrin, Enhanced corrosion resistance of Mg alloy ZK60 after processing by integrated extrusion and equal channel angular pressing, Acta Mater. 59 (2011) 6176–6186, doi:10.1016/j.actamat.2011.06.033.
[17] C. Op't Hoog, N. Birbilis, Y. Estrin, Corrosion of pure Mg as a function of grain size and processing route, Adv. Eng. Mater. 10 (2008) 579–582, doi:10.1002/adem.200800046.
[18] K. Sun, H. Gao, J. Hu, Y. Yan, Effect of pH on the corrosion and crack growth behavior of the ZK60 magnesium alloy, Corros. Sci. 179 (2020) 109135, doi:10.1016/j.corsci.2020.109135.
[19] L.J. Liu, M. Schlesinger, Corrosion of magnesium and its alloys, Corros. Sci. 51 (2009) 1733–1737, doi:10.1016/j.corsci.2009.04.025.
[20] W. Xu, N. Birbilis, G. Sha, Y. Wang, J.E. Daniels, Y. Xiao, M. Ferry, A high-specific-strength and corrosion-resistant magnesium alloy, Nat. Mater. 14 (2015) 1229–1235, doi:10.1038/nmat4435.
[21] J. Huang, G.L. Song, A. Atrens, M. Dargusch, What activates the Mg surface - a comparison of Mg dissolution mechanisms, J. Mater. Sci. Technol. 57 (2020) 204–220, doi:10.1016/j.jmst.2020.03.060.
[22] A. Tahara, T. Kodama, Potential distribution measurement in galvanic corrosion of Zn/Fe couple by means of kelvin probe, Corros. Sci. 42 (2000) 655–673, doi:10.1016/S0010-938X(99)00074-8.
[23] K.B. Deshpande, Numerical modeling of micro-galvanic corrosion, Electrochim. Acta 56 (2011) 1737–1745, doi:10.1016/j.electacta.2010.09.044.
[24] G. Song, B. Johannesson, S. Hapugoda, D. St John, Galvanic corrosion of magnesium alloy AZ91D in contact with an aluminium alloy, steel and zinc, Corros. Sci. 46 (2004) 955–977, doi:10.1016/S0010-938X(03)00190-2.
[25] E. Mccafferty, Calculation of current distribution in circular corrosion cells, Corros. Sci. 16 (1996) 183–190, doi:10.1016/0010-938X(76)90060-3.
[26] N. Birbilis, G. Williams, K. Gusieva, A. Samaniego, M.A. Gibson, H.N. McMurray, Poisoning the corrosion of magnesium, Electrochem. Commun. 34 (2013) 295–298, doi:10.1016/j.elecom.2013.07.021.
[27] A. Samaniego, K. Gusieva, I. Llorente, S.F. Jr, N. Birbilis, Exploring the possibility of protective surface oxides upon Mg alloy AZ31 via lutetium additions, Corros. Sci. 89 (2014) 101–110, doi:10.1016/j.corsci.2014.08.015.
[28] C.Q. Li, D.K. Xu, X. Chen, B.J. Wang, R.Z. Wu, E.H. Han, N. Birbilis, Composition and microstructure dependent corrosion behavior of Mg-Li alloys, Electrochim. Acta 260 (2018) 55–64, doi:10.1016/j.electacta.2017.11.091.
[29] S. Hong, F. Zheng, G. Shi, J. Li, X. Luo, F. Xing, L. Tang, B. Dong, Determination of impressed current efficiency during accelerated corrosion of reinforcement, Cem. Concr. Compos. 108 (2020) 103536, doi:10.1016/j.cemconcomp.2020.103536.
[30] M. Grimm, A. Lohmüller, R.F. Singer, S. Virtanen, Influence of the microstructure on the corrosion behavior of cast Mg-Al alloys, Corros. Sci. 155 (2019) 195–208, doi:10.1016/j.corsci.2019.04.024.

[31] Q. Jiang, D. Lu, N. Wang, X. Wang, J. Zhang, The corrosion behavior of Mg-Nd binary alloys in the harsh marine environment, J. Magnes. Alloy (2020), doi:10.1016/j.jma.2019.12.010.
[32] P. Wu, F. Xu, K. Deng, F. Han, Z. Zhang, R. Gao, Effect of extrusion on corrosion properties of Mg-2Ca-xAl (x = 0, 2, 3, 5) alloys, Corros. Sci. 127 (2017) 280–290, doi:10.1016/j.corsci.2017.08.014.
[33] G.Z. Meng, C. Zhang, Y.F. Cheng, Effects of corrosion product deposit on the subsequent cathodic and anodic reactions of X-70 steel in near-neutral pH solution, Corros. Sci. 50 (2008) 3116–3122, doi:10.1016/j.corsci.2008.08.026.
[34] G. Song, A.L. Bowles, D.H. Stjohn, Corrosion resistance of aged die cast magnesium alloy AZ91D, Mat. Sci. Eng. A 366 (2004) 74–86, doi:10.1016/j.msea.2003.08.060.
[35] D. Song, A.B. Ma, J. Jiang, P. Lin, D. Yang, J. Fan, Corrosion behavior of equal-channel-angular-pressed pure magnesium in NaCl aqueous solution, Corros. Sci. 52 (2010) 481–490, doi:10.1016/j.corsci.2009.10.004.
[36] K.D. Ralston, D. Fabijanic, N. Birbilis, Effect of grain size on corrosion of high purity aluminium, Electrochim. Acta 56 (2011) 1729–1736, doi:10.1016/j.electacta.2010.09.023.
[37] J.G. Speight, Lange's Handbook of Chemistry, 17th ed., McGraw Hill, New York, 2016.
[38] C.L. Yaws, Yaws' Handbook of Properties of the Chemical Elements, Knovel, New York, 2011.
[39] F. Cao, Z. Shi, G. Song, M. Liu, A. Atrens, Corrosion behavior in salt spray and in 3.5% NaCl solution saturated with $Mg(OH)_2$ of as-cast and solution heat-treated binary Mg-X alloys: x = Mn, Sn, Ca, Zn, Al, Zr, Si, Sr, Corros. Sci. 76 (2013) 60–97, doi:10.1016/j.corsci.2013.06.030.
[40] H. Ha, J. Kang, J. Yang, C. Dong, B. Sun, Limitations in the use of the potentiodynamic polarisation curves to investigate the effect of Zn on the corrosion behavior of as-extruded Mg-Zn binary alloy, Corros. Sci. 75 (2013) 426–433, doi:10.1016/j.corsci.2013.06.027.
[41] X. Liu, D. Shan, Y. Song, E. Han, Influence of yttrium element on the corrosion behaviors of Mg-Y binary magnesium alloy, J. Magnes. Alloy 5 (2017) 26–34, doi:10.1016/j.jma.2016.12.002.
[42] Z. Shi, F. Cao, G. Song, M. Liu, A. Atrens, Corrosion behavior in salt spray and in 3.5% NaCl solution saturated with $Mg(OH)_2$ of as-cast and solution heat-treated binary Mg-RE alloys: RE = Ce, La, Nd, Y, Gd, Corros. Sci. 76 (2013) 98–118, doi:10.1016/j.corsci.2013.06.032.
[43] M. Esmaily, J.E. Svensson, S. Fajardo, N. Birbilis, G.S. Frankel, S. Virtanen, R. Arrabal, S. Thomas, L.G. Johansson, Progress in materials science fundamentals and advances in magnesium alloy corrosion, Prog. Mater. Sci. 89 (2017) 92–193, doi:10.1016/j.pmatsci.2017.04.011.
[44] A. Srinivasan, S. Ningshen, U. Kamachi Mudali, U.T.S. Pillai, B.C. Pai, Influence of Si and Sb additions on the corrosion behavior of AZ91 magnesium alloy, Intermetallics 15 (2007) 1511–1517, doi:10.1016/j.intermet.2007.05.012.
[45] T. Zhang, Y. Shao, G. Meng, Z. Cui, F. Wang, Corrosion of hot extrusion AZ91 magnesium alloy: i-relation between the microstructure and corrosion behavior, Corros. Sci. 53 (2011) 1960–1968, doi:10.1016/j.corsci.2011.02.015.
[46] A. Soltan, M.S. Dargusch, Z. Shi, D. Gerrard, A. Atrens, Understanding the corrosion behavior of the magnesium alloys EV31A, WE43B, and ZE41A, Mater. Corros. 70 (2019) 1527–1552, doi:10.1002/maco.201910845.
[47] O. Gaon, G. Dror, O. Davidi, A. Lugovskoy, The effect of the local microstructure of MRI 201S magnesium alloy on its corrosion rate, Corros. Sci. 93 (2015) 167–171, doi:10.1016/j.corsci.2015.01.018.
[48] Z. Shi, A. Atrens, An innovative specimen configuration for the study of Mg corrosion, Corros. Sci. 53 (2011) 226–246, doi:10.1016/j.corsci.2010.09.016.
[49] Z. Qiao, Z. Shi, N. Hort, N.I.Z. Abidin, A. Atrens, Corrosion behavior of a nominally high purity Mg ingot produced by permanent mould direct chill casting, Corros. Sci. 61 (2012) 185–207, doi:10.1016/j.corsci.2012.04.030.
[50] F. Cao, Z. Shi, J. Hofstetter, P.J. Uggowitzer, G. Song, M. Liu, A. Atrens, Corrosion of ultra-high-purity Mg in 3.5% NaCl solution saturated with $Mg(OH)_2$, Corros. Sci. 75 (2013) 78–99, doi:10.1016/j.corsci.2013.05.018.
[51] C. Zhang, L. Wu, H. Liu, G. Huang, B. Jiang, A. Atrens, F. Pan, Microstructure and corrosion behavior of Mg-Sc binary alloys in 3.5 wt.% NaCl solution, Corros. Sci. 174 (2020) 108831, doi:10.1016/j.corsci.2020.108831.
[52] H.Y. Ha, J.Y. Kang, S.G. Kim, B. Kim, S.S. Park, C.D. Yim, B.S. You, Influences of metallurgical factors on the corrosion behavior of extruded binary Mg-Sn alloys, Corros. Sci. 82 (2014) 369–379, doi:10.1016/j.corsci.2014.01.035.
[53] R. Arrabal, A. Pardo, M.C. Merino, M. Mohedano, P. Casajús, K. Paucar, G. Garcés, Effect of Nd on the corrosion behavior of AM50 and AZ91D magnesium alloys in 3.5 wt.% NaCl solution, Corros. Sci. 55 (2012) 301–312, doi:10.1016/j.corsci.2011.10.033.
[54] S. Baek, H. Ju, H. Young, S. Sohn, H. Shin, K. Choi, K. Lee, J. Gu, C. Dong, B. Sun, H. Ha, S. Soo, Effect of alloyed Ca on the microstructure and corrosion properties of extruded AZ61 Mg alloy, Corros. Sci. 112 (2016) 44–53, doi:10.1016/j.corsci.2016.07.011.
[55] J. Jayaraj, S.A. Raj, A. Srinivasan, S. Ananthakumar, U.T.S. Pillai, N. Gopala, K. Dhaipule, U.K. Mudali, Composite magnesium phosphate coatings for improved corrosion resistance of magnesium AZ31 alloy, Corros. Sci. 113 (2016) 104–115, doi:10.1016/j.corsci.2016.10.010.
[56] H.Y. Choi, W.J. Kim, The improvement of corrosion resistance of AZ91 magnesium alloy through development of dense and tight network structure of Al-rich a phase by addition of a trace amount of Ti, J. Alloy. Compd. 696 (2017) 736–745, doi:10.1016/j.jallcom.2016.11.215.
[57] S. Baek, J. Su, H. Shin, C. Dong, B. Sun, Role of alloyed Y in improving the corrosion resistance of extruded Mg-Al-Ca-based alloy, Corros. Sci. 118 (2017) 227–232, doi:10.1016/j.corsci.2017.01.022.
[58] D. Li, H. Wang, D. Wei, Z. Zhao, Y. Liu, Effects of deformation texture and grain size on corrosion behavior of Mg-3Al-1 Zn alloy sheets, ACS Omega 5 (2020) 1448–1456, doi:10.1021/acsomega.9b03009.
[59] C. Zhang, L. Wu, G. Huang, Y. Huang, B. Jiang, Effect of microalloyed Ca on the microstructure and corrosion behavior of extruded Mg alloy AZ31, J. Alloy. Compd. 823 (2020) 153844, doi:10.1016/j.jallcom.2020.153844.
[60] Z. Zhang, G. Wu, A. Atrens, W. Ding, Influence of trace As content on the microstructure and corrosion behavior of the AZ91 alloy in different metallurgical conditions, J. Magnes. Alloy 8 (2020) 301–317, doi:10.1016/j.jma.2019.12.004.
[61] S. Kyu, C. Blawert, K.A. Yasakau, S. Yi, N. Scharnagl, B. Suh, Y. Min, B. Sun, C. Dong, Effects of combined addition of Ca and Y on the corrosion behaviors of die-cast AZ91D magnesium alloy, Corros. Sci. 166 (2020) 108451, doi:10.1016/j.corsci.2020.108451.
[62] Y. Luo, Y. Deng, L. Guan, L. Ye, X. Guo, The microstructure and corrosion resistance of as-extruded Mg-6Gd-2Y-(0-1.5)Nd-0.2Zr alloys, Mater. Des. 186 (2020) 108289, doi:10.1016/j.matdes.2019.108289.
[63] M. Esmaily, D.B. Blücher, J.E. Svensson, M. Halvarsson, L.G. Johansson, New insights into the corrosion of magnesium alloys–The role of aluminum, Scr. Mater. 115 (2016) 91–95, doi:10.1016/j.scriptamat.2016.01.008.
[64] B. Homayun, A. Afshar, Microstructure, mechanical properties, corrosion behavior and cytotoxicity of Mg-Zn-Al-Ca alloys as biodegradable materials, J. Alloy. Compd. 607 (2014) 1–10, doi:10.1016/j.jallcom.2014.04.059.
[65] F. Tong, X. Chen, Q. Wang, S. Wei, W. Gao, Hypoeutectic Mg-Zn binary alloys as anode materials for magnesium-air batteries, J. Alloy. Compd. 857 (2021) 157579, doi:10.1016/j.jallcom.2020.157579.
[66] P. Cao, M. Qian, D.H. Stjohn, Effect of manganese on grain refinement of Mg-Al based alloys, Scr. Mater. 54 (2006) 1853–1858, doi:10.1016/j.scriptamat.2006.02.020.
[67] K. Gusieva, C.H.J. Davies, J.R. Scully, N. Birbilis, Corrosion of magnesium alloys: the role of alloying, Int. Mater. Rev. 60 (2015) 169–194, doi:10.1179/1743280414Y.0000000046.
[68] Y. Hou, P. Zhou, B. Yu, T. Zhang, F. Wang, The dual role of Mg^{2+} in the conversion bath during the treatment of magnesium alloys: the completing effect between heterogeneous nucleation and crystal growth, Electrochim. Acta 388 (2021) 138568, doi:10.1016/j.electacta.2021.138568.